

**Properties of a thermoplastic composite skin-stiffener interface in a stiffened structure manufactured by laser-assisted tape placement with in situ consolidation**

Bandaru, Aswani Kumar; Clancy, Gearóid; Peeters, Daniël; O'Higgins, Ronan M.; Weaver, Paul M.

**DOI**

[10.1016/j.compstruct.2019.02.011](https://doi.org/10.1016/j.compstruct.2019.02.011)

**Publication date**

2019

**Document Version**

Accepted author manuscript

**Published in**

Composite Structures

**Citation (APA)**

Bandaru, A. K., Clancy, G., Peeters, D., O'Higgins, R. M., & Weaver, P. M. (2019). Properties of a thermoplastic composite skin-stiffener interface in a stiffened structure manufactured by laser-assisted tape placement with in situ consolidation. *Composite Structures*, 214, 123-131.  
<https://doi.org/10.1016/j.compstruct.2019.02.011>

**Important note**

To cite this publication, please use the final published version (if applicable).  
Please check the document version above.

**Copyright**

Other than for strictly personal use, it is not permitted to download, forward or distribute the text or part of it, without the consent of the author(s) and/or copyright holder(s), unless the work is under an open content license such as Creative Commons.

**Takedown policy**

Please contact us and provide details if you believe this document breaches copyrights.  
We will remove access to the work immediately and investigate your claim.

## **Properties of a thermoplastic composite skin-stiffener interface in a stiffened structure manufactured by laser-assisted tape placement with in-situ consolidation**

Aswani Kumar Bandaru<sup>1</sup>, Gearóid Clancy<sup>1</sup>, Daniël Peeters<sup>1,2</sup>, Ronan M. O' Higgins<sup>1\*</sup> and Paul M. Weaver<sup>1</sup>

<sup>1</sup>Irish Centre for Composites Research (IComp), Bernal Institute, School of Engineering, University of Limerick, Ireland

<sup>2</sup>Faculty of Aerospace Engineering, Delft University of Technology, Kluyverweg 1, Delft 2629HS, The Netherlands

\*Email: [ronan.ohiggins@ul.ie](mailto:ronan.ohiggins@ul.ie)

**Keywords:** Automated Fibre Placement; Thermoplastic; Mechanical testing; Interface Properties

### **ABSTRACT**

A critically important consideration of stiffened structural panels is the interfacial properties between skin and stiffener. In the present study a novel implementation of laser-assisted tape placement (LATP) was used to produce a representative skin-stiffener of a wingbox from carbon fibre reinforced PEEK. First, a stiffener is manufactured using this method and subsequently the skin is attached using the same method without need for a secondary bonding process. The interfacial properties between the skin and stiffener have been characterised in terms of interlaminar shear strength (ILSS) and fracture toughness (Mode-I and Mode-II) properties. LATP laydown direction and laser power was found to influence the skin-stiffener interface Mode-I fracture toughness, but not affect the Mode-II fracture toughness. The values of ILSS and fracture toughness compare favourably with those results reported in the literature, in particular for those reported for equivalent aerospace certified CF/PEEK material (APC-2).

### **1. INTRODUCTION**

Interest in thermoplastic composites continues to increase due to their potential for fast forming and weldability, as well as for their superior fracture toughness and excellent fire/smoke/toxicity (FST) properties compared with thermoset composites. With increasing demand for higher production through-put, out-of-autoclave (OOA) methods for composite structure processing are of increasing interest for the aerospace industry. Laser-assisted automated tape placement (LATP) in-situ consolidation of fibre reinforced thermoplastic composite material has the potential to produce high quality components without the requirement for a secondary consolidation processing step. Research has focused on the implementation of the LATP process as a replacement for

conventional manufacturing techniques [1-3]. Recently, a large complex wingbox demonstrator with integrated stiffeners was produced from carbon fibre (CF) reinforced polyether ether ketone (PEEK) using this process without the need for a secondary consolidation process [4]. This work implemented a number of innovations, including: the use of fibre steering to produce a variable angle tow (VAT) laminate to increase the skin buckling load and also to blend in-plane stiffnesses between different components (skin, web and stiffener); a unitized structure was produced by in-situ consolidation and in-situ joining of the stiffeners as part of the laser consolidation process. However, the formation of a good interlaminar bond during the process is a major concern due to the short time available for intimate contact development and polymer healing. The aim of this study is to examine the bond performance between the demonstrator skin and reinforcing stiffeners.

The bond strength and interlaminar fracture toughness of composite laminates can be characterised using short beam interlaminar shear strength (ILSS), double cantilever beam (DCB) and end-notched flexure (ENF) tests [5]. Grouve et al. [6] performed mandrel peel tests to measure the degree of bonding in carbon fibre (CF)/polyphenylene sulfide (PPS) composites processed by LAMP. The bonding strength was quantified through interfacial fracture toughness. Good bonding was observed for low laser input power at relatively fast lay down rates. Comer et al. [7] evaluated the performance of CF/PEEK composites by performing wedge peel and ILSS tests. The toughness of LAMP processed laminates were compared with those manufactured by autoclave consolidation. While the autoclave processed specimens exhibited the highest strength, the interlaminar toughness was found to be dependent on the processing parameters that affected the level of crystallinity in the PEEK. Stokes-Griffin et al. [8] studied the influence of temperature and placement rate on ILSS of CF/PEEK composites; it was found to be independent of process temperature at 100 mm/s up to a temperature of 550°C. Beyond this temperature, ILSS properties degraded. Many other researchers also reported the short beam strength of CF/PEEK composites which are produced from heat press [9], autoclave [7,10] and autoclave re-consolidation of ATP [3,11].

For CF reinforced epoxy composites, typical reported  $G_{Ic}$  values are around 260 J/m<sup>2</sup> [12]. Higher fracture toughness performance is expected from thermoplastic composites; reported  $G_{Ic}$  values for CF/PEEK range from 1.2-2.5 kJ/m<sup>2</sup> [13]. Gao and Kim [14] observed that a faster cooling rate decreases the interfacial bond strength. A slow cooling rate improves the bond strength, while fast cooling enhanced the ductility of PEEK, which increased the fracture toughness. This implies that the bond strength and fracture toughness can be changed relative to each other. The influence of cooling rate on the fracture toughness of CF/PEEK prepreg tapes was also reported in [15]; the fracture toughness increases at faster cooling rates. It was concluded that

higher cooling rates which increase polymer ductility are beneficial for fracture toughness. A study of fracture toughness of CF/PEEK processed by autoclave and LATP [13] concluded that the fracture toughness of LATP samples was almost 38% higher than the autoclave specimens. LATP samples had a more amorphous interlaminar bondline, due to the temperature profile experienced during processing and significant plastic deformation in interior plies. In a study of the influence of processing parameters on CF/PEEK [16], it was found that Mode-I fracture toughness was dominated by matrix properties, while Mode-II energy release rate was dependent on the bond strength between fibre and matrix. A study of the influence of specimen thickness and span length on Mode-II response of CF/PEEK [17], determined that Mode-II toughness was independent of thickness at a span length to thickness ratio greater than 20. In all of the studies reported, the characterisation specimens were manufactured in a single process. No data for larger representative structures was presented. Published data on the interfacial characterisation of CF/PEEK is very limited, in particular for LATP processed laminates.

In this study, a unitized demonstrator wingbox was produced from CF/PEEK using the LATP process, details of which are given in the companion paper [4]. The completed demonstrator wingbox is shown in Fig.1. Joining of skin and stiffener directly as part of the LATP process without any adhesives or rivets is a key achievement of the present work. However, it is essential to know the interface toughness and bond strength of the integrated skin-stiffener. A representative skin-stiffener was manufactured using the same approach as used for processing the wingbox demonstrator. The interfacial properties were characterised using ILSS, Mode-I (DCB) and Mode-II (ENF) fracture toughness tests. Two different processing strategies were adopted for manufacturing the DCB and ENF specimens. Firstly, the crack is located along the manufacturing (CAM) direction, i.e. the direction in which the tape was laid down, and then secondly the crack lies opposite to the manufacturing (COM) direction. Mode-I and mode-II fracture toughness values were obtained for both CAM and COM specimens. The influence of the manufacturing process on the fracture toughness results were then analysed.

## **2. EXPERIMENTAL METHODS**

For manufacturing the skin-stiffener laminates, the tape used was supplied by Toho Tenax (carbon fibre (Tenax -E IMS65 24 K)/PEEK). The width of the tape was 6.35 mm and the thickness was 0.18 mm. The laminate was manufactured at a laydown speed of 3m/min. A schematic diagram of the LATP method used to process the representative skin-stiffener is shown in Fig.2. The LATP system at the University of Limerick consists of a LATP head attached to the KUKA robot arm (KR240 L210-2) which was supplied by AFPT GmbH. The target

temperature was set to 400°C. During manufacturing, the laser power was controlled using a temperature feedback loop; the nip-point (i.e., the point where the roller presses down the incoming tape on the substrate) temperature was monitored with an infra-red (IR) camera. The laser angle relative to the substrate was set before each layer such that the focus of the laser was close to the nip-point. The laser spot size was 20 mm wide in the tape direction and 40 mm along the length of the tape. The pneumatic pressure on the compaction cylinder was set to 2.5bar. The roller used was a conformable silicone roller, provided by AFPT. Fibre reinforced thermoplastic tapes bond with the substrate under the application of heat, provided by the laser, and pressure, provided by the LATP head roller. A detailed description of the LATP process can be found in [8, 18]. The steps carried out for the manufacture of test specimens are described in following sub-sections.

### ***2.1. Manufacturing of skin-stiffener for ILSS tests***

For the ILSS specimens, a stiffener was manufactured (Fig.3a) and a representative skin layer (Fig.3b) was subsequently laid-up over this. Steel box sections were placed at each side of the stiffener to support it. These were shimmed to ensure that the bonding surface was flush with the surrounding tool surface. The box section had a 100mm nominal width, allowing only a relatively short run-up length for the skin laminate process. As the CF/PEEK tape does not adhere to steel, a strip of double-sided adhesive (Fig.3) was used to prevent the tape from slipping during placement. CF/PEEK tapes with a unidirectional (UD) stacking sequence was used for both the skin and stiffener ( $[0^\circ]_8$  each), so that the ILSS specimens harvested would correctly adhere to the lay-up recommended in the ASTM standard [19].

### ***2.2. Manufacturing of DCB and ENF test specimens***

To manufacture DCB and ENF test specimens representative of the interface between a skin and stiffener, a  $[0^\circ]_8$  flat laminate was manufactured and cut into sections. A brass plate of the same thickness was inserted between the sections to simulate the mould surface between stiffeners. A  $[0^\circ]_8$  skin layer was then laid-up over this assembly. Polyimide film strips, 50 mm in length, were placed at the mid-plane of the specimens to simulate a crack in the laminate, as shown in Fig.4. The LATP head laser is controlled by a temperature feedback loop from an infra-red (IR) camera. Due to the difference thermal emissivity of material surfaces, the laser power fluctuates when moving from one material surface to another as it tries to stabilise on the desired feedback temperature from the camera. The first brass plate was 150 mm long to allow the LATP laser power to stabilise. For the first two laminates, the polyimide film was located at the finish, as the bond strength at the start may be affected by the laser power fluctuation as it moves from the brass plate to the composite surface. On the

third laminate, the polyimide film was placed at the start to evaluate what effect laser power fluctuation has on the initial bond strength.

The manufacturing set-up can be seen in Fig.5a. The brass and composite plates were secured in place by adhesive tape. Due to the build-up of thermal stresses during lay-up caused by consolidation temperature tape being laid on a cooling substrate, warping (spring back) occurred across the width of the laminate can be seen in Fig.5c. However, as the width of the specimens to be harvested are small relative to the curvature of the panel (25 mm for DCB and ENF; 10 mm for ILSS), the influence of the on the test results should be negligible.

### **2.3. Mechanical characterisation of bond strength**

Mechanical tests were performed to evaluate the bond strength between the skin and stiffener, manufactured using a novel LATP approach. All specimens were harvested using a diamond blade cutter taking precautions not to induce delamination.

#### **2.3.1. ILSS characterisation**

Interlaminar shear strength (ILSS) tests were carried out according to ASTM D2344 [19]. Specimens were cut to the dimensions: 20 x 10 mm<sup>2</sup>. Tests were performed with a Tinius Olsen H25KS test machine with a load cell of 1 kN (expected accuracy of 0.5%). As shown in Fig.6, the specimen was placed on two cylindrical supports of 3 mm diameter and a 6 mm diameter cylindrical head was used to apply the load at a rate of 1 mm/min until the first failure occurred. Laminate warping (spring back) caused issues with specimens harvesting, reducing the number of valid specimens available for testing to four, rather than five as recommended by the standard [19].

ILSS,  $\sigma_s$ , was calculated using:

$$\sigma_s = \frac{3P_{max}}{4bh} \quad (1)$$

where:  $P_{max}$  is the maximum load obtained from test,  $b$  is the width and  $h$  is the thickness of the specimen.

#### **2.3.2. DCB and ENF characterisation**

For DCB and ENF characterisation, the specimens were prepared according to ASTM D5528 [20] and ASTM D7905 [21], respectively. Tests were performed with a Tinius Olsen H25KS test machine with a load cell of 1 kN (expected accuracy of 0.5%). Four samples were considered for each test. A schematic of the crack locations in different Bays and manufacturing direction are shown in Fig.4b.

The size of the DCB specimens was 130 mm x 25 mm x 3.5 mm with an initial nominal delamination length of 44 mm. In the case of DCB test specimens, loading blocks of 25 mm x 12.5 mm were adhered to the specimens using an adhesive. The load was applied at a displacement rate of 2.5 mm/min. The DCB test set-up is shown in Fig.7a. Calibration markings were made along the thickness of the specimens from the crack tip to capture the

propagation of the delamination. A digital camera was used to record crack propagation and these images were successively used to measure the crack length. Mode-I fracture toughness,  $G_{Ic}$ , was calculated using modified beam theory [20] as

$$G_{Ic} = \frac{3P\delta}{2b(a + |\Delta|)} \quad (2)$$

where:  $P$  is the load,  $\delta$  is the load point displacement,  $b$  is the width,  $a$  is the delamination length.  $\Delta$  was determined experimentally by generating a least squares plot of cube root of compliance ( $C^{1/3}$ ), as a function of delamination length. The compliance  $C$ , is the ratio of load point displacement to the load ( $\delta/P$ ).

The ENF tests were carried out according to ASTM D7905 [21]. The specimens were placed on cylindrical rollers of 5 mm and a roller of 6mm diameter was placed on the top centre of the specimen. A span of 80mm was used for this test. Markings were made on the specimen as shown in Fig.7b, which assist in the visual detection of the delamination tip and in making the compliance calibration (CC). The edges were marked with three vertical CC markings, within the expected crack region, at distances of 20 mm, 30 mm and 40 mm from the tip of the insert. Loading was applied under displacement control at a rate of 0.5 mm/min for all CC markings. Mode-II fracture toughness,  $G_{IIc}$ , was calculated using the CC method from:

$$G_{IIc} = \frac{3mP_{max}^2 a_0}{2b} \quad (3)$$

where:  $P_{max}$  is the maximum load from the test,  $a_0$  is the crack length used in the fracture test and  $b$  is the specimen width.  $m$  was determined using least square analysis of the compliance versus crack length cubed ( $a^3$ ).

### 3. RESULTS AND DISCUSSION

The interfacial properties of LATP manufactured skin-stiffener was obtained through different mechanical tests and the results are presented in this section. Typical load-displacement curves are shown for ILSS tests, while load-displacement and resistance (R) curves (toughness vs delamination length) are presented for the DCB and ENF tests. Fractography analysis of the failure mechanisms for each test is also presented.

#### 3.1. ILSS characteristics of skin-stiffener

The ILSS tests were performed on UD skin-stiffener specimens; the results were compared with the existing literature. The ILSS load-displacement response, shown in Fig.8, can be divided into three stages; Stage-I exhibits a linear elastic response up to a displacement of 0.7 mm. For Stage-II, the load reaches a maximum and plateaus with increasing displacement. In Stage-III, the load decreases gradually exhibiting progressive failure of the specimen. Similar behaviour for UD ILSS load-displacement for carbon fibre/PEEK was reported in the literature [7].

The ILSS data obtained for CF/PEEK material in this study is compared with values reported in the literature for existing aerospace grade material (APC-2) in Fig. 9. Specimen preparation in the current study is different from that reported in the literature. The bonding of the skin-stiffener in the present study was achieved using LATP in-situ consolidation. In the literature presented each ILSS characterisation laminate was manufactured in a single process. The average ILSS value obtained in the current study (47.4MPa) is higher than the average ILSS value reported (43.1MPa). Agarwal et al. [23] reported an ILSS of  $50 \pm 2.25$ MPa with laser-assisted filament winding which is 5.2% higher than that achieved in this study. Though the span-to-thickness ratio of both studies is the same, the consolidation temperature was higher (475°C), compared to the current work (400 °C). This consolidation temperature difference, in combination with a winding approach, which generally assists in reducing laminate springback, may have aided the achievement of the higher ILSS value. Tierney and Gillespie [3] used a gas heated ATP system to manufacture APC-2 laminates for testing. Gas heated systems usually fully melt the tape and the heat is transferred by convection, rather than radiation for the LATP system. For comparable lay-down speeds, the current study achieved a 13.8% higher ILSS value. However, higher values of ILSS in [3] were achieved at much slower laydown rates. Rosselli and Santare [24] achieved 46MPa at a relatively slow laydown rate of 1.2m/min for curved ILSS specimens. Similarly, Mazumdar and Hoa [22] reported the ILSS of 35.7MPa for curved specimens. In both of these studies, the specimens were harvested from a ring winding of 146mm diameter with an approximate thickness of 5mm. While the ILSS specimens were slightly curved, the span-to-thickness ratio was similar to the present work, so a reasonably valid comparison can be made. Considering that the LATP process used in this study has not been optimised for the material system investigated, the data obtained compares well with the ILSS values reported in the literature [3, 22-24]. Different failure modes that occurred in the skin-stiffener are shown in Fig.10. The specimens exhibited a clear interlaminar shear failure and plastic deformation; delamination occurred at either the top or bottom outermost layers, but no delamination was observed at the skin-stiffener interface, indicating a good interface bond.

### *3.2. DCB results or Mode-I fracture toughness results*

Representative DCB test load-displacement curves are shown in Fig.11. The initial loading stage is linearly increased until the crack initiates, the load then drops steadily as the crack propagates. The load-displacement curve exhibits 'saw-tooth' behaviour associated with stick-slip crack propagation. This stick-slip behaviour is attributed to regions of varying toughness in the specimens [5, 25]. The load drops abruptly as the crack propagates rapidly, after which the load increases again with displacement until the load drops again due to

further unstable crack propagation. A significant difference was observed between the CAM and COM load-displacement response. The CAM DCB specimens achieved a significantly higher crack initiation load relative to the COM specimens.

The resistance curves of CAM and COM specimens for a typical DCB test are shown in Fig.12; the first digit in the specimen code indicates from which manufacturing bay it was harvested (see Fig.5). Significant scatter was observed for all specimens. The initial stage was characterized by an increase in  $G_{Ic}$  values with crack length. Examination of the DCB specimens showed that fibre bridging occurred in the crack tip opening area (Fig.12b), which helped to increase the  $G_{Ic}$  values. The initial fracture toughness of CAM samples (Fig.12) exceeds that of COM samples (Fig.12). Examination of the laser power plots for the manufacturing process indicates that this is caused by the variation in the laser power, affecting nip point temperature, during processing. On the LATP system, the laser power is controlled by a feedback loop from an Infra-red (IR) camera which measures nominal temperature at the nip point. However, as the laser passes over materials of different emissivity, the IR temperature reading changes causing the laser power to fluctuate. The power as a function of time is shown in Fig.13. The power traces are averaged over 5 points before and after the actual point to smooth the data. Each line represents a different track of the panel during manufacturing. At the first brass insert, the laser power started at 550-580W and reduced linearly to 490-520W, over 70 mm or 1.4s, giving a power loss slope of approximately 42.9 W/s. For the second brass insert an initial laser power of 490W to 530W at the start, reducing linearly to 420-460W, giving a similar power loss slope ( $\approx 42.9$  W/s). At the final brass insert, the initial power was similar to the second brass insert at 490-530W, the plot then exhibited a fluctuation spike, before the power loss slope follows a similar trend to the other brass inserts, reducing to 425-465W. The power spike may have been due to some oxidation or tape residue on the surface of the brass insert. In the case of polyimide inserts, at both the first and second inserts, the power decreased from 540-580W to 490-530W, with a drop of 50 W which occurred very suddenly (power loss slope  $\approx 100$ W/s). For the third polyamide tape, there was too much scatter to say anything useful in terms of numbers, but in this case, an increase in power occurred. The reason for the drop and increase in the power is most likely the temperature sensor picking up the brass plate (decrease) or the composite part (increase), which have a different emissivity coefficient, which is not taken into account during manufacture.

Laser power plots for Bay 1 show that the laser power remains relatively consistent across the bay, particularly passing from the composite to the polyimide tape, i.e. the crack initiation point for the DCB specimens. The time taken to reach a steady state in Bay 1 was about 0.3 sec, or 15 mm and in bay 2 it was about 0.45 seconds,

or 22 mm. However, this was towards the end of the sample, so likely only influences the final fracture of the sample. Looking from the crack tip, the power was constant. Bay 1 specimens exhibit the highest  $G_{Ic}$  values, with initial crack initial starting at above  $1\text{kJ/m}^2$ , and rising rapidly to plateau above  $2.3\text{kJ/m}^2$ . For Bay 2, the laser power is less stable, increasing steadily over the bay to the composite/polyimide interface. For the Bay 2 DCB specimens, the  $G_{Ic}$  values increase to approximately  $1.5\text{kJ/m}^2$  near crack initiation, but decrease steadily in line with the laser power decrease away from the composite/polyimide interface. For Bay 3, the power was constant from the start, towards the end it started decreasing, approximately 0.4 seconds, or 20 mm, before the start of the brass plate. At the start, some scatter was observed in the power plot, which could explain (part of) the scatter in these results. The Bay 3 specimens achieved the worst initial  $G_{Ic}$  values (below  $0.5\text{kJ/m}^2$ ), but increased steadily to approximately  $2.0\text{kJ/m}^2$  as the crack progressed. For all other cases, the power only decreases towards the end of the sample, so its influence should be limited to the fracture toughness in the last 20 mm of the sample.

The laser power plot shows that there is a significant power fluctuation across the polyimide/composite interface, but it begins to stabilise and increase across the bay. This data indicates that the laser power/processing temperature significantly influences the interface bond, but more research is required to determine the exact mechanism by which the bond is affected.

An overview of the Mode-I fracture toughness of integrated skin-stiffener (CAM and COM samples) are presented in Table 1. This  $G_{Ic}$  behaviour is similar to that reported in other studies [13,15,16,27] and the values obtained compare well with the values of carbon fibre/PEEK composites reported previously (see Table 1).

Fig. 14 shows the laser power as a function of crack length. In this figure, thick lines represent the average laser power over all tracks laid down for each bay and dashed lines represent minimum and maximum values of power at each point. On the x-axis, from 0 to 50 mm represents the length of the polyimide tape insert. From Fig. 12, it is observed that the  $G_{Ic}$  of Bay-1 and Bay-3 follow a similar trend of increasing toughness. However, there is a significant difference in values of fracture energy between them due to the change in the mean power at the start of each bay. In addition, the difference in the minimum power along the tracks is larger. From Fig. 14, it is also clear that Bay-3 initially has greater laser power scatter resulting in lower fracture energy values at crack initiation. The large difference in the laser power traces at the crack initiation point of Bay-2 and Bay-3 corresponds with the trend in the fracture energy values.

A representative DCB specimen fracture surface is shown in Fig. 15a. Unlike the fracture surface obtained in [13] for autoclave consolidated CF/PEEK, which exhibited grey zones for crack initiation and dark zones for

crack growth, the surfaces obtained in the current study do not exhibit any significant difference on the fracture surface. However, all the specimens exhibited fibre bridging after crack initiation as shown in Fig.15b.

### 3.3. ENF results or Mode-II fracture toughness results

Representative load-displacement curves for CAM and COM ENF test specimens are shown in Fig.16. Similar load-displacement response was observed for CAM and COM specimens, indicating that the ENF Mode II response is constant from beginning to the end of the interface. All specimens exhibited initial linear behaviour, followed by a change in the load-displacement response indicating crack initiation. The crack propagation was stable for each specimen. The response of the current ENF specimens is similar to that reported in the literature [17, 28]. Mode-II fracture toughness was evaluated based on the compliance calibration method outlined in ASTM D7905 [21]. Fig.17 shows the compliance of ENF specimens versus crack length for both CAM and COM specimens. The results revealed that the compliance of all specimens increases linearly with respect to the crack length. The direction of manufacturing did not show any influence on the compliance. This response of the Mode-II ENF skin-stiffeners compliance represents the bending stiffness of the specimens [27]. The  $G_{IIc}$  values of CAM and COM specimens varied from 1.35 kJ/m<sup>2</sup> to 2.84 kJ/m<sup>2</sup>. The average values of  $G_{IIc}$  for CAM and COM samples were 1.88±0.66 kJ/m<sup>2</sup> and 1.78±0.35 kJ/m<sup>2</sup>, respectively. The values obtained are in agreement with ENF carbon fibre/PEEK values previously reported [17].

## 4. CONCLUSIONS

A representative skin-stiffener of a stiffened structure (wingbox) was manufactured from CF/PEEK using LATP in-situ consolidation. The skin and stiffener were joined together as part of the LATP layup process without need for secondary processing. The purpose of this study was to assess the bond strength achieved at the skin-stiffener interface by characterizing the bond using ILSS, DCB and ENF tests. In the case of the ILSS tests, specimens exhibited a clear interlaminar shear failure, but delamination occurred at either the top or bottom outermost layers, with no delamination observed at the skin-stiffener interface, indicating a good interface bond. Mode-I fracture tests revealed that the laser power exhibited a significant influence on the fracture toughness of the skin-stiffener interface. However, Mode-II test results were more consistent and did not seem to be affected by laser power fluctuation. More research is required to determine the exact mechanism by which the bond is affected by the laser power/processing temperature. In addition, the processing parameters for the material tapes used in this study have not been optimised, so further work is required to optimise the process.

The results show that the LATP manufacturing process for the skin-stiffener produced a bond at the interface that was comparable with that reported in the literature for similar in-situ consolidation methods. In addition, the

values obtained compared well with the properties of certified aerospace grade materials (APC-2) reported in the literature. While the processing parameters for this manufacturing method are not fully optimised, this data suggests that the material and processes used in the present study can be developed for implementation in aerospace structures.

## **ACKNOWLEDGEMENTS**

This project has received funding from the EI and from the European Union's Horizon 2020 research and innovation programme under the Marie-Sklodowska Curie grant agreement No 713654.

The authors also would like to thank Science Foundation Ireland (SFI) for funding Spatially and Temporally VARIABLE COMPOSITE Structures (VARICOMP) Grant No. (15/RP/2773) under its Research Professor programme.

The authors would also like to thank Irish Composites Centre (IComp) for its help with the LATP.

## **References**

1. Sonmez FO, Hahn HT. Analysis of on-line consolidation process in thermoplastic composite tape placement. *J Thermo Compos Mater* 1997;10:543-72.
2. Schledjewski R, Latrille M. Processing of unidirectional fiber reinforced tapes—fundamentals on the way to a process simulation tool (prosimfrt). *Compos Sci Technol* 2003;63(14):2111–8.
3. Tierney J, Gillespie Jr JW. Modeling of in situ strength development for the thermoplastic composite tow placement process. *J Compos Mater* 2006;40(16):1487–506.
4. Oliveri, Vi; D. Peeters, ; G.J. Clancy, D. Jones, R.M. O'Higgins, P.M. Weaver, , Design, manufacture and test of an in-situ consolidated carbon fiber-reinforced PEEK variable stiffness, unitized wingbox, 2018 *AIAAJournal*, (Accepted, in-press DOI: 10.2514/1.J057758)
5. Reis, P.N.B., Ferreira, J.A.M., Costa, J.D.M., Pereira, A., “Interlaminar fracture in woven carbon-epoxy laminates,” *Fracture and Structural integrity related issues*, Vol. 30, 2014, pp.431-437.
6. Groupe, W. J. B., Warnet, L. L., Rietman, B., Visser, H. A., Akkerman, R., “Optimization of the tape placement process parameters for carbon–PPS composites,” *Composites Part A: Applied Science and Manufacturing*, Vol. 50, 2013, pp. 44-53.
7. Comer, A. J, D. Ray, W.O. Obande, D. Jones, J. Lyons, I. Rosca, R.M. O'Higgins, and M.A. McCarthy. “Mechanical characterisation of carbon fibre–PEEK manufactured by laser-assisted automated-tape-placement and autoclave,” *Composites Part A: Applied Science and Manufacturing*, Vol. 69, 2015, pp. 10-20.

8. Stokes-Griffin, C. M., Compston, P., "The effect of processing temperature and placement rate on the short beam strength of carbon fibre-PEEK manufactured using a laser tape placement process," *Composites Part A: Applied Science and Manufacturing*, Vol. 78, 2015, pp. 274-283.
9. Mantell, S. C., Springer, G. S., "Manufacturing process models for thermoplastic composites," *Journal of Composite Materials*, Vol. 26, No. 16, 1992, pp. 2348-2377.
10. Schledjewski, R., Miaris, A., "Thermoplastic tape placement by means of diode laser heating," *Proceedings of International SAMPE symposium and exhibition*, Vol.54; 2009.
11. Khan, M. A., Mitschang, P., Schledjewski, R., "Identification of some optimal parameters to achieve higher laminate quality through tape placement process," *Advanced Polymer Technology*, Vol. 29, No. 2, 2010, pp. 98-111.
12. Chen, J.H., Schulz, E., Bohse, J., Hinrichsen, G., "Effect of fibre content on the interlaminar fracture toughness of unidirectional glass-fibre/polyamide composite," *Composites Part A: Applied Science and Manufacturing*, Vol. 30, 1999, pp. 747-755.
13. Ray, D., A.J. Comer, J. Lyons, W. Obande, D. Jones, R.M.O. Higgins, and M.A. McCarthy Fracture toughness of carbon fiber/polyether ether ketone composites manufactured by autoclave and laser-assisted automated tape placement. *Journal of Applied Polymer Science*, 2015. 132(11): p. 1-10..
14. Gao, S. L., and Kim, J. K., "Cooling rate influences in carbon fibre/PEEK composites. Part 1. Crystallinity and interface adhesion," *Composites Part A: Applied Science and Manufacturing*, Vol. 31 (6), 2000, pp. 517-530.
15. Gao, S. L., and Kim, J. K., "Cooling rate influences in carbon fibre/PEEK composites. Part II: interlaminar fracture toughness," *Composites Part A: Applied Science and Manufacturing*, Vol. 32 (6), 2001, pp. 763-774.
16. Vu-Khanh, T., and Frikha S., "Influence of Processing on Morphology, Interface, and Delamination in PEEK/Carbon Composites," *Journal of Thermoplastic Composite Materials*, Vol. 12, 1999, pp. 84-95.
17. Davies, P., "Influence of ENF specimen geometry and friction on the mode II delamination resistance of Carbon/PEEK," *Journal of Thermoplastic Composite Materials*, Vol 10, 1997, pp. 353-361.
18. Frketic, J., Dickens, T., and Ramakrishnan S., "Automated manufacturing and processing of fibre-reinforced polymer (FRP) composites: An additive review of contemporary and modern techniques for advanced materials manufacturing," *Additive Manufacturing*, Volume 14, 2017, Pages 69-86.

19. ASTM D2344., "Standard Test Method for Short-Beam Strength of Polymer Matrix Composite Materials and Their Laminates," 2016.
20. ASTM D5528., "Standard Test Method for Mode I Interlaminar Fracture Toughness of Unidirectional Fibre-Reinforced Polymer Matrix Composites," 2013.
21. ASTM D7905., "Standard Test method for Determination of the Mode II Interlaminar Fracture Toughness of Unidirectional Fibre-Reinforced Polymer Matrix Composites," 2014.
22. Mazumdar, S. K., and Hoa, S. V., "Application of Taguchi method for process enhancement of on-line consolidation technique," *Composites*, Vol. 26, 1995, pp. 669-673.
23. Agarwal, V., McCullough, R. L., Schultz, J. M., "The Thermoplastic Laser-Assisted Consolidation Process-Mechanical and Microstructure Characterization," *Journal of Thermoplastic Composite Materials*, Vol. 9, 1996, pp. 365-380.
24. Rosselli, F., and Santare, M. H., "Comparison of the short beam shear (SBS) and interlaminar shear device (ISD) tests," *Composites Part A: Applied Science and Manufacturing*, Vol. 28A, 1997, pp. 587-594.
25. Matsuda, S., Hojo, M., Ochiai, S., Murakami, A., Akimoto, H., Ando, M., Effect of ionomer thickness on mode I interlaminar fracture toughness for ionomer toughened CFRP. *Compos. Part A-Appl. S.*, 30 (1999) 1311-1319.
26. Z. Qureshi, T. Swait, R. Scaife, H.M. El-Dessouky, In situ consolidation of thermoplastic prepreg tape using automated tape placement technology: Potential and possibilities, *Composites Part B: Engineering*, Volume 66, 2014, Pages 255-267.
27. Moghadam, B.A., and Taheri, F., "Influence of graphene nanoplatelets on Modes I, II and III interlaminar fracture toughness of fibre-reinforced polymer composites," *Engineering Fracture Mechanics*, Vol. 143, 2015, pp. 97-107.
28. Sacchetti, F., et al., "Interlaminar fracture toughness of 5HS Carbon/PEEK laminates. A comparison between DCB, ELS and mandrel peel tests," *Polymer Testing*, Volume 66, 2018, Pages 13-23.

## Tables

**Table 1:** Mode-I fracture energy of integrated skin-stiffener with respect to crack length

Crack length (mm)	$G_{Ic}$ (kJ/m <sup>2</sup> )			Literature
	CAM Samples		COM Samples	
	Bay-1	Bay-2	Bay-3	
44.75	1.17±0.11	0.79±0.18	0.26±0.15	1.20-2.50 [13, 15] Nominal crack length = 50mm
45.75	1.26±0.09	1.03±0.14	0.30±0.14	
46.75	1.52±0.11	1.09±0.18	0.43±0.13	
47.75	1.78±0.13	1.10±0.18	0.52±0.16	
48.75	1.88±0.16	1.17±0.16	0.56±0.18	
58.75	2.07±0.11	1.52±0.05	1.12±0.14	
68.75	2.18±0.10	1.48±0.10	1.36±0.14	
78.75	2.32±0.19	1.30±0.08	1.58±0.09	
88.75	2.38±0.16	1.20±0.17	1.79±0.15	
98.75	2.47±0.19	1.00±0.12	1.81±0.12	

Note: ± indicates the standard deviation

## Figure Titles

**Figure 1:** Representative wing box with skin-stiffener.

**Figure 2:** Schematic of LATP method.

**Figure 3:** Skin-stiffener for ILSS test: (a) set-up for laying the skin on stiffener, and (b) laying of the first layer of skin on the stiffener

**Figure 4:** Schematic of the manufacturing approach for DCB and ENF tests, (a) the plan view of the initial substrate set-up and (b) a side view of the final lay-up including crack locations. Bay 1 and 2 CAM and Bay 3 COM. *(all dimensions in mm)*

**Figure 5:** Set-up for manufacturing of skin-stiffener for DCB and ENF tests: (a) composite laminate with brass plates (b) extra layers laid down (c) final panel

**Figure 6:** Typical test set-up for ILSS and the test specimen.

**Figure 7:** Fracture toughness characterisation: (a) Mode I DCB; (b) Mode II ENF.

**Figure 8:** ILSS specimen load-displacement response for representative skin-stiffeners.

**Figure 9:** Comparison of ILSS.

**Figure 10:** Interlaminar shear failure of skin-stiffener.

**Figure 11:** Representative load-displacement responses from CAM and COM DCB specimens.

**Figure 12:** Representative Mode-I fracture toughness vs. crack length curves for Bays 1-3.

**Figure 13:** Laser power as a function of time.

**Figure 14:** Laser power as a function of crack length, thick lines represent the average laser power, while dashed lines represent minimum and maximum laser power values.

**Figure 15:** Mode-I fracture of integrated skin-stiffener.

**Figure 16:** Typical load vs. displacement of ENF specimens.

**Figure 17:** Compliance of ENF specimens.

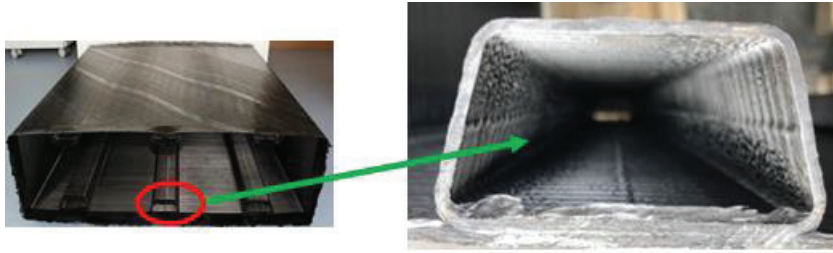


**Figure 1:** Representative wing box with skin-stiffener.

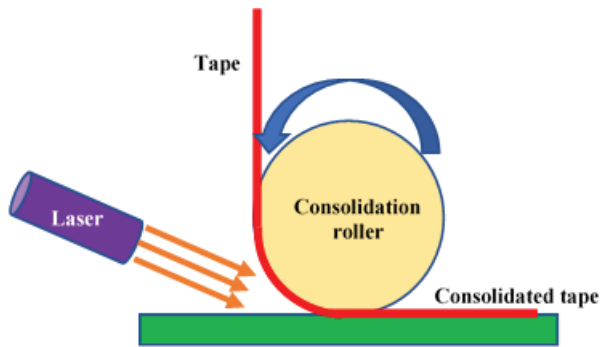


**Figure 2:** Schematic of LATP method.

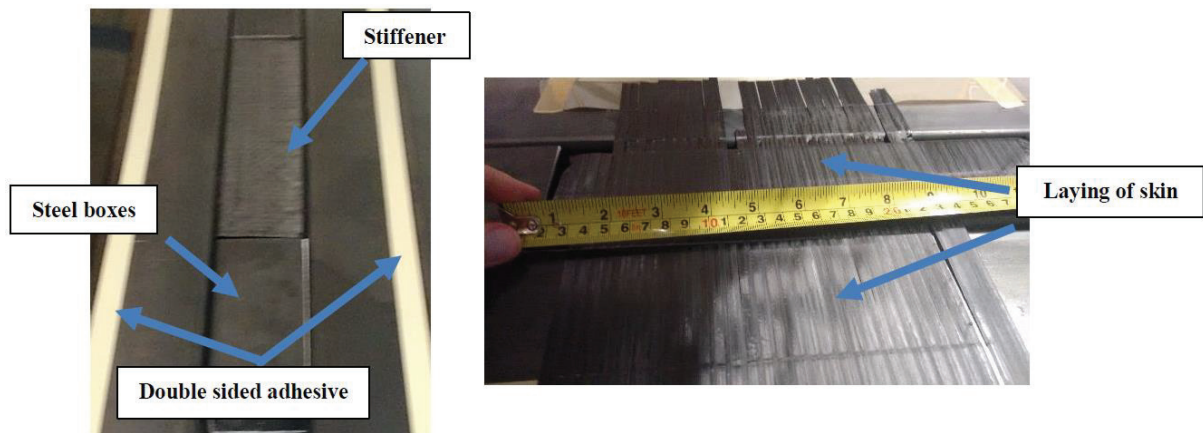


**Figure 3:** Skin-stiffener for ILSS test: (a) set-up for laying the skin on stiffener, and (b) laying of the first layer of skin on the stiffener

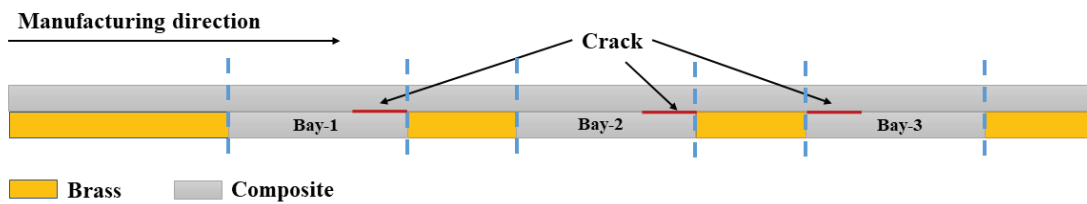
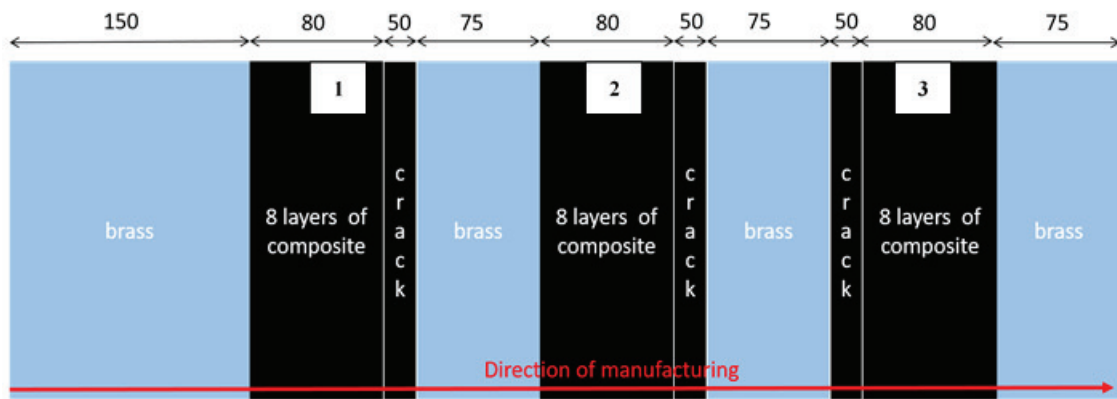


**Figure 4:** Schematic of the manufacturing approach for DCB and ENF tests, (a) the plan view of the initial substrate set-up and (b) a side view of the final lay-up including crack locations. Bay 1 and 2 CAM and Bay 3 COM. (all dimensions in mm)

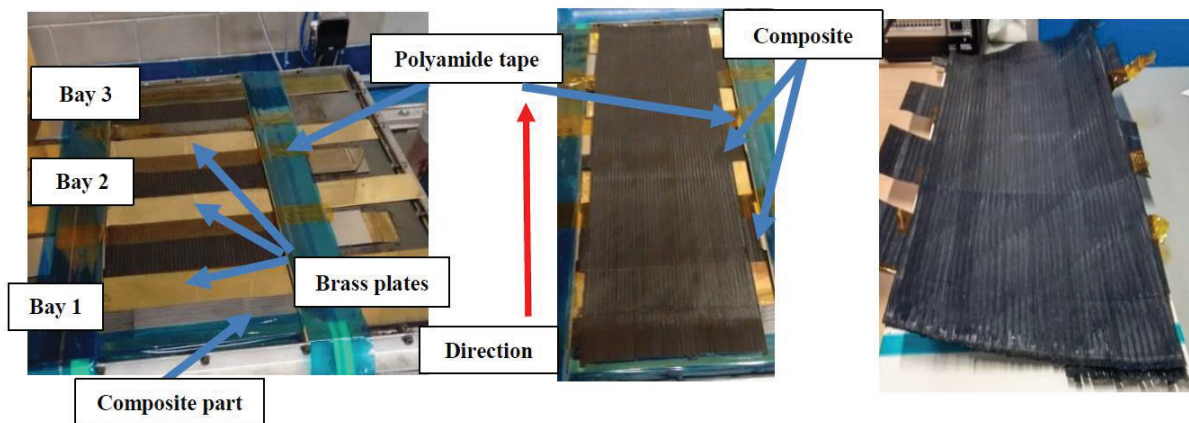


**Figure 5:** Set-up for manufacturing of skin-stiffener for DCB and ENF tests: (a) composite laminate with brass plates (b) extra layers laid down (c) final panel

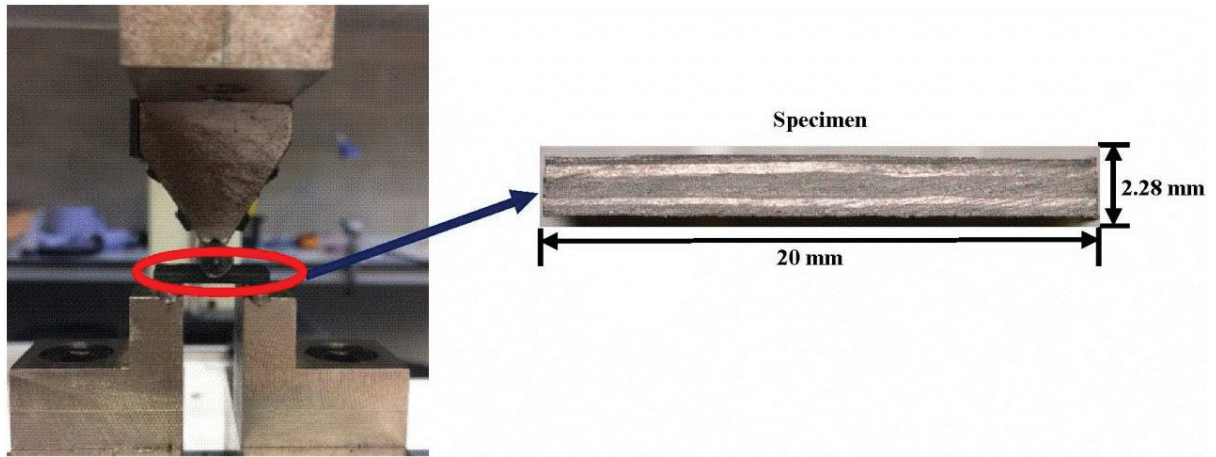


**Figure 6:** Typical test set-up for ILSS and the test specimen.

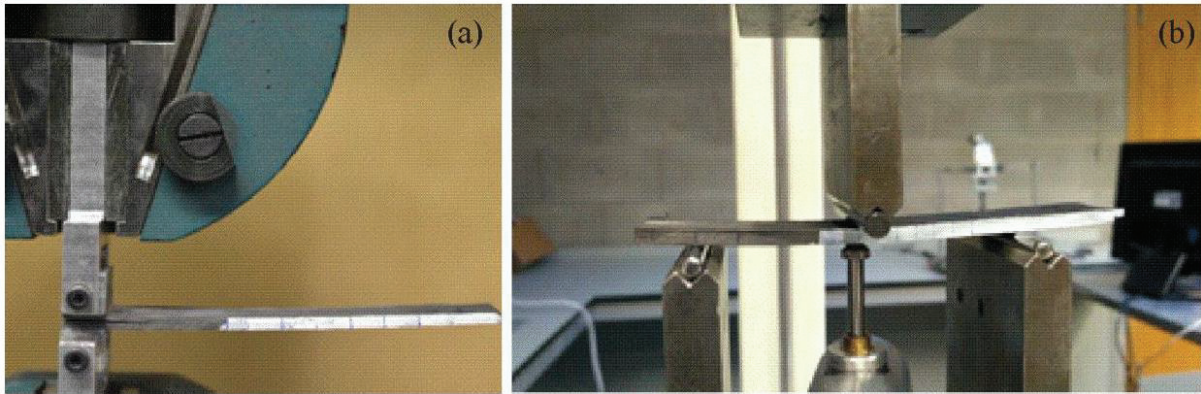


**Figure 7:** Fracture toughness characterisation: (a) Mode I DCB; (b) Mode II ENF.

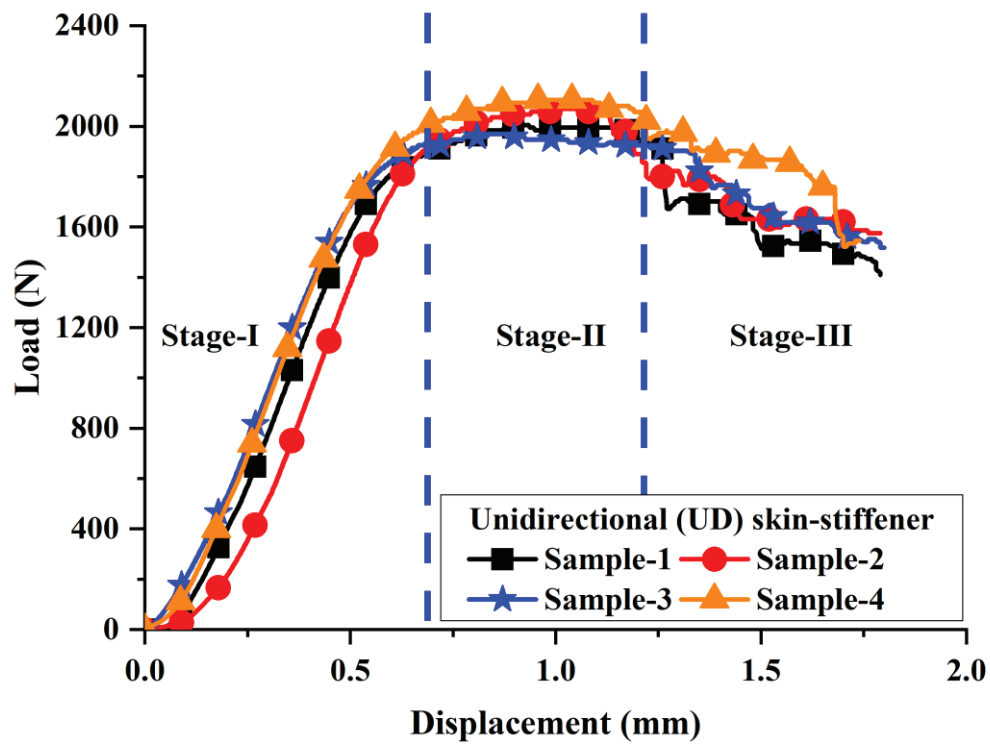


Figure 8: ILSS specimen load-displacement response for representative skin-stiffeners.

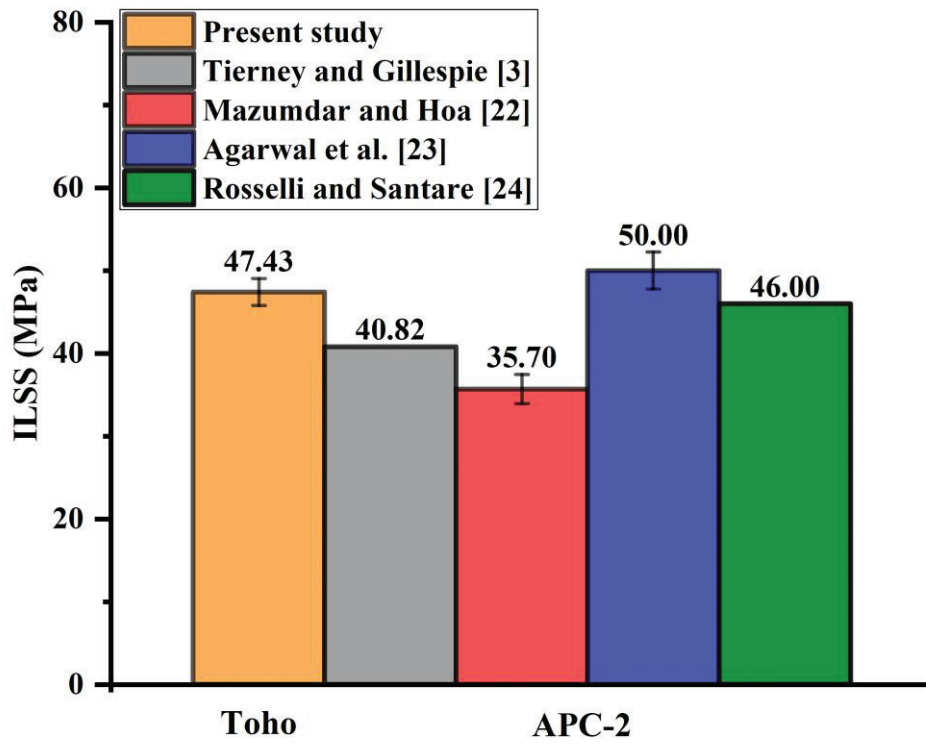


Figure 9: Comparison of ILSS.

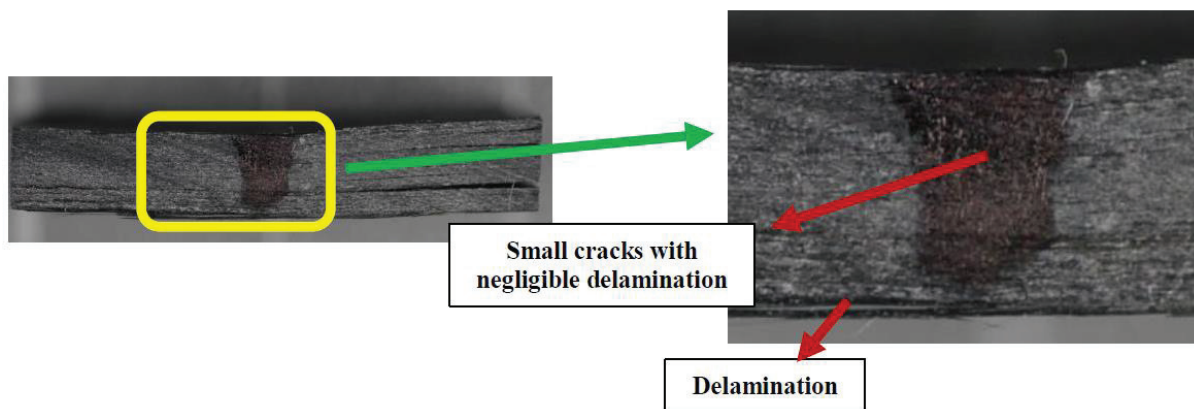


Figure 10: Interlaminar shear failure of skin-stiffener.

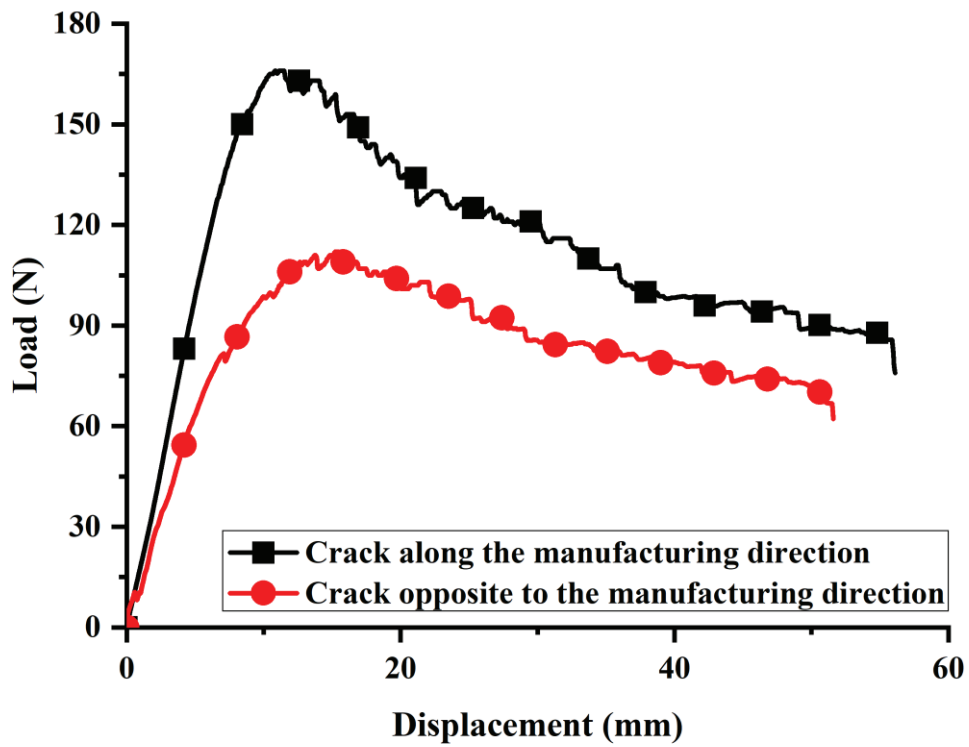


Figure 11: Representative load-displacement responses from CAM and COM DCB specimens.

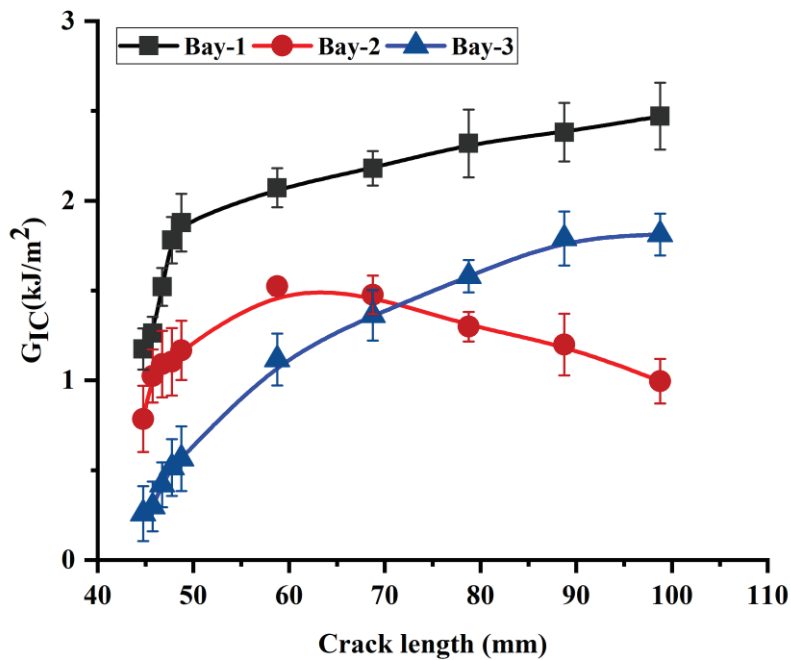


Figure 12: Representative Mode-I fracture toughness vs. crack length curves for Bays 1-3.

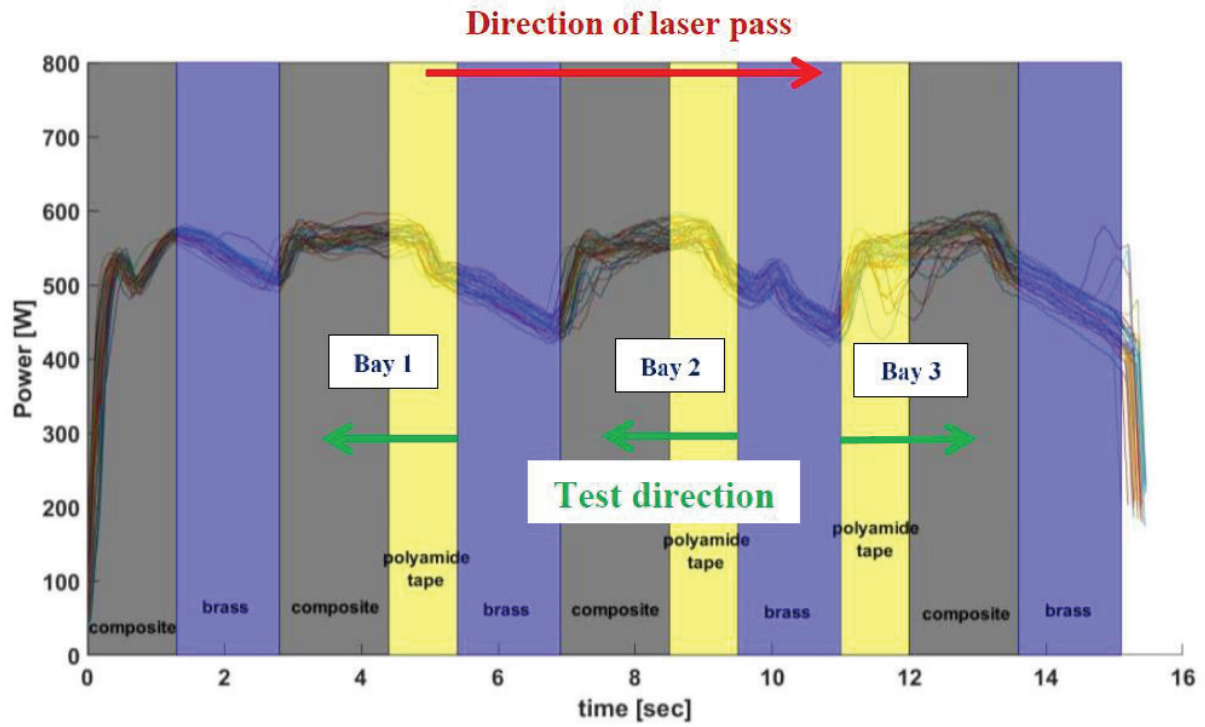


Figure 13: Laser power as a function of time.

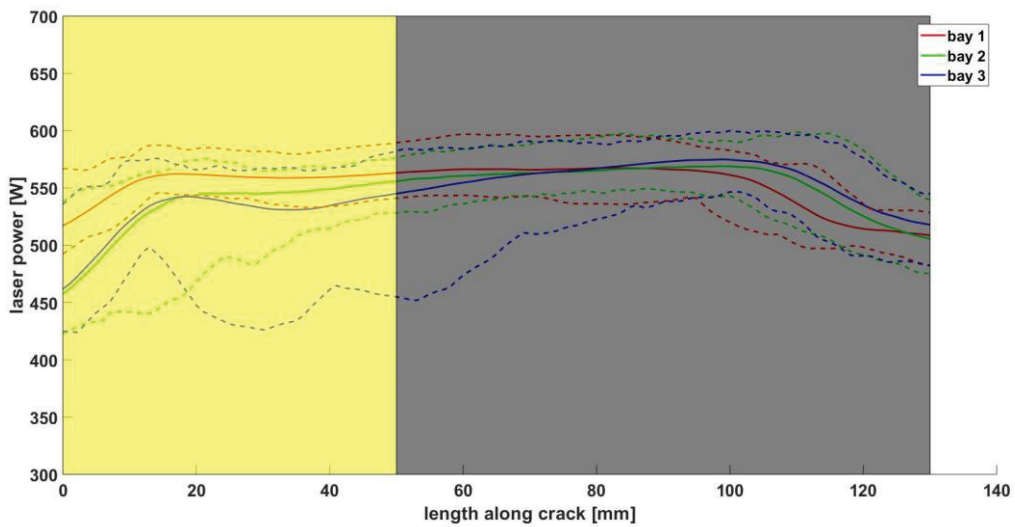


Figure 14: Laser power as a function of crack length, thick lines represent the average laser power, while dashed lines represent minimum and maximum laser power values.

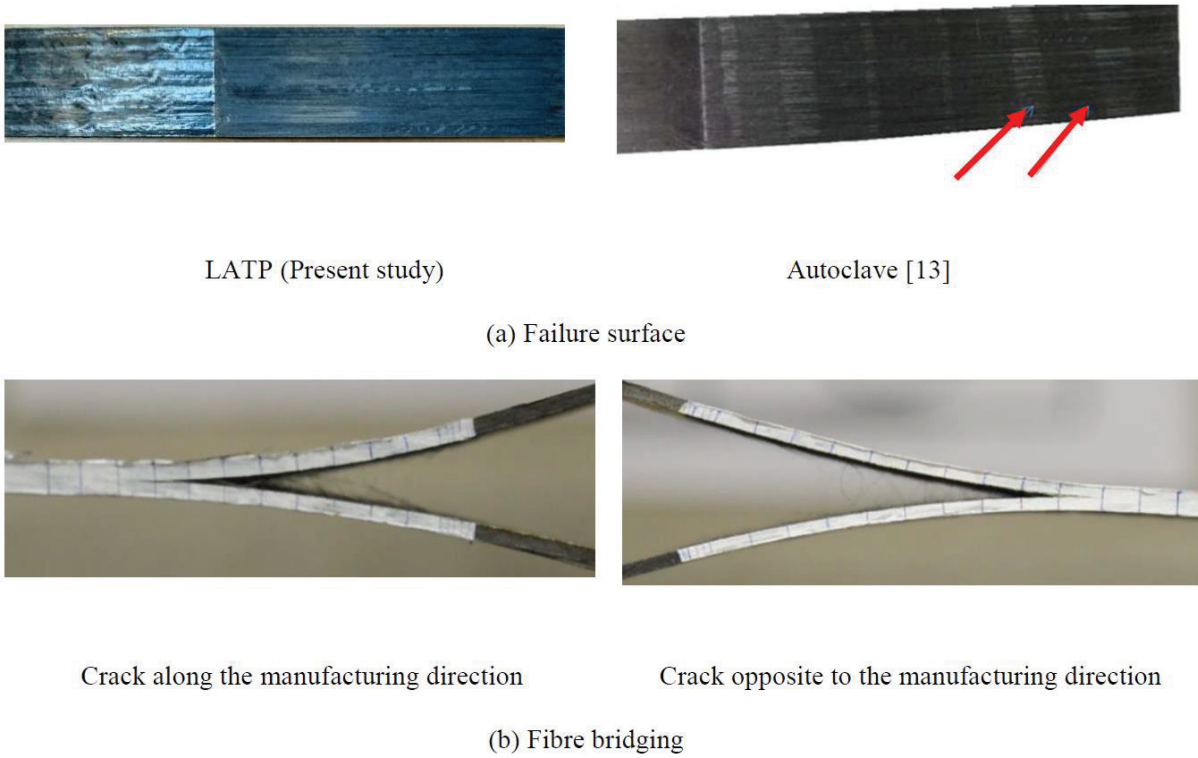


Figure 15: Mode-I fracture of integrated skin-stiffener.

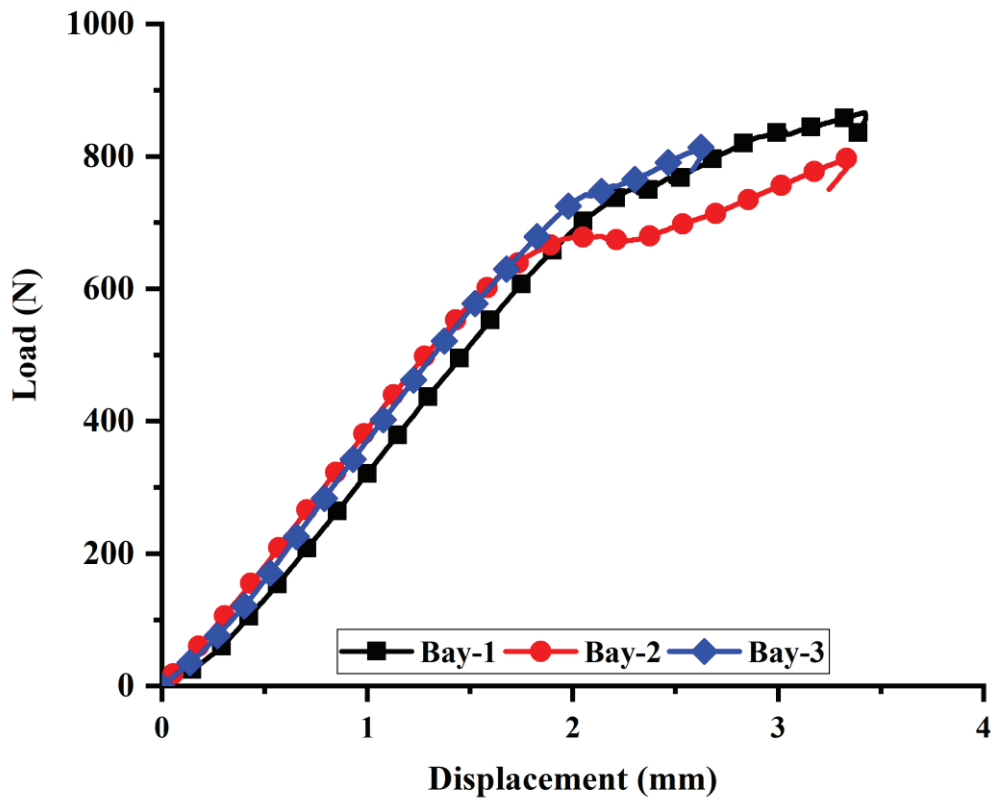


Figure 16: Typical load vs. displacement of ENF specimens.

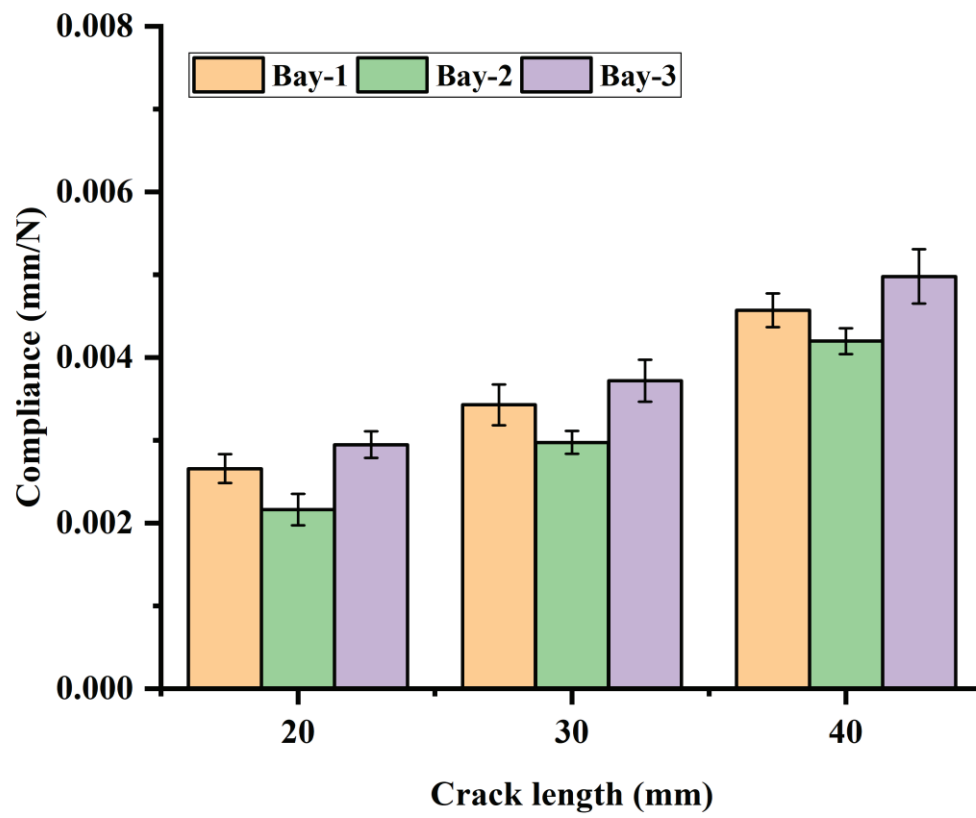


Figure 17: Compliance of ENF specimens.